Induced Optical Activity of DNA-templated Cyanine Dye Aggregates: Exciton Coupling Theory and TD-DFT Studies.

ARTICLE *in* THE JOURNAL OF PHYSICAL CHEMISTRY A · JULY 2013

Impact Factor: 2.69 · DOI: 10.1021/jp309807y · Source: PubMed

4 AUTHORS, INCLUDING:

Michal Maj
Korea University
8 PUBLICATIONS **27** CITATIONS
SEE PROFILE

Robert W. Góra
Wroclaw University of Technology
54 PUBLICATIONS **718** CITATIONS
SEE PROFILE

Minhaeng Cho
IBS, Korea University
217 PUBLICATIONS **7,484** CITATIONS
SEE PROFILE

THE JOURNAL OF PHYSICAL CHEMISTRY A

Article

pubs.acs.org/JPCA

Induced Optical Activity of DNA-Templated Cyanine Dye Aggregates: Exciton Coupling Theory and TD-DFT Studies

Michał Maj,[†] Jonggu Jeon,[†] Robert W. Góra,[‡] and Minhaeng Cho*[,†,§]

[†]Department of Chemistry, Korea University, Seoul 136-701, Korea

[‡]Theoretical Chemistry Group, Institute of Physical and Theoretical Chemistry, Wrocław University of Technology, Wybrzeże Wyspiańskiego 27, 50-370 Wrocław, Poland

[§]Multidimensional Spectroscopy Laboratory, Korea Basic Science Institute, Seoul 136-713, Korea

ABSTRACT: Certain cyanine dye molecules have been observed to self-assemble in DNA templates to form large chiral aggregates, which exhibit induced circular dichroism. The structure and circular dichroism (CD) of one such system, aggregates of a cationic $DiSC_2(5)$ cyanine dye, are investigated using the time-dependent Kohn−Sham density functional theory (TD-DFT) and exciton coupling model. A series of TD-DFT calculations on the aggregates with one, two, and four dye molecules clearly shows the onset of CD induced by the helically twisted structure compatible with the minor groove of DNA templates. More simplified exciton coupling model analysis successfully reproduces the major positive Cotton effect observed in the experiment as well as the TD-DFT calculations, but it is unable to capture minor features of the CD spectrum that are closely related to absolute configurations of constituent dyes in the complex. We assess the performance of various methods used for evaluation of the electronic coupling energies between interacting chromophores. Our results confirm that the interchromophore interactions in cyanine dye aggregates are primarily electrostatic in nature and indicate that the exciton coupling model is adequate for studying induced CD of self-assembled aggregates of cyanine dye molecules.

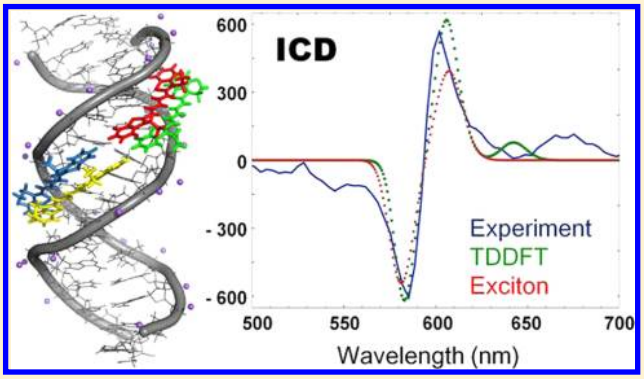

I. INTRODUCTION

Cyanine dyes exhibit large extinction coefficients and moderate quantum yields resulting in bright fluorescence signals and hence widespread potential applications. Among others, their complexes with DNA and RNA exhibit interesting photophysical properties leading to their practical applications as fluorescent probes. Recently, it has been shown that cyanine dye molecules can spontaneously form an aggregate on DNA templates, forming self-assembled supramolecular helical structures that exhibit induced chirality and, consequently, induced circular dichroism (CD) as well as other interesting optical properties.[1,2]

Recently, we carried out femtosecond optical activity (both CD and optical rotatory dispersion (ORD)) measurements of the cyanine dye complexes binding to the minor groove of a short double-helical DNA oligonucleotide.[3,4] Not only because the cyanine molecules in the aggregate on the DNA template are arranged in a helical configuration but also because their electronic transitions are coupled to form a delocalized exciton manifold, the aggregate exhibits induced optical activity and its CD and ORD spectra provide information on the strength of electronic couplings and the 3D structure of the helical aggregate. Using a broadband laser pulse and employing a self-heterodyne-detection method,[3−7] we were able to measure the spectral interferograms resulting from the interference between the local oscillator field and chiral free-induction-decay field emitted by the DNA-templated cyanine dye aggregates.[8] The standard Fourier-transform spectral interferometry procedure[9] was used to convert the measured spectral interferograms to the CD and ORD spectra.

In the present work, we study one of such complex, namely, a symmetrical cationic 3,3′-diethylthiadicarbocyanine ($DiSC_2(5)$) dye binding to a DNA minor groove. A detailed spectroscopic analysis of this system was reported by Seifert et al.,[1] which revealed both a spontaneous dimerization of dye molecules in the vicinity of alternating adenine-thymine (AT) or inosine-cytosine (IC) residues and a formation of extended helical aggregates consisting of $DiSC_2(5)$ dimers in an end-to-end alignment. Although the structure and the mechanism of formation of these complexes have been studied, a detailed theoretical investigation to characterize the structure, excitonic nature, and chiroptical properties of this system has not been performed yet. Nonetheless, Tomlinson et al.[10] made the first attempt to study its structure using the intermediate neglect of

Special Issue: Prof. John C. Wright Festschrift

Received: October 4, 2012
Revised: November 16, 2012
Published: November 26, 2012

differential overlap (INDO) single configuration interaction (SCI) semiempirical method.[11]

In this contribution, we shall present results of quantum chemistry calculations on the structure and excitonic coupling constants as well as numerically simulated UV−vis absorption, CD, and ORD spectra of the coupled helical $DiSC_2(5)$ aggregates. The structure of DNA−tetrameric cyanine dye complex was obtained from molecular dynamics (MD) simulation, and it was used as the initial configuration for subsequent ab initio calculations using a variety of computational approaches for estimation of the coupling constants among the chromophores. We have employed three different methods for the evaluation of interchromophore electrostatic couplings based on the transition densities of isolated dye molecules obtained within adiabatic time dependent density functional theory (TD-DFT): the transition charge from electrostatic potential (TrESP), the transition density cube (TDC), and the fragment excitation difference (FED) methods. The calculated coupling constants obtained with these methods were then used to build an exciton model of the system, which was in turn used to calculate the absorption, CD, and ORD spectra of the complex. To assess the accuracy of the exciton model, we also performed TD-DFT calculations on the selected cyanine dye aggregates. Thus, we can directly compare the results of the exciton model calculations of induced CD and ORD spectra with our experimental spectra as well as those from electronic structure calculations. We shall present a discussion on the advantage of the simplified exciton model as well as its limitation.

II. COMPUTATIONAL METHODS

A. Structure of Cyanine Dye Aggregate. In order to obtain a good initial structure for subsequent QM structure optimization, we carried out a series of MD simulations of the AT-10 DNA duplex (a double helix with 5 repeating AT units per strand) with four $DiSC_2(5)$ molecules inserted into its minor groove. The preliminary DNA structure had been generated using the NUCGEN[12] routine of the AMBER[13] package and equilibrated to ensure a stable structure before inserting the dye molecules. Then, an MD simulation was carried out for 5 ns in NVT ensemble followed by 20 ns in NPT ensemble with a time step of 1 fs in each run. All the simulations were carried out using the AMBER package with ff09 force field[14] and a flexible TIP3P[15] potential for water molecules. The Langevin thermostat was applied to equilibrate the system at 300 K. The particle mesh Ewald (PME) summation method[16] for treatment of long-range electrostatic interactions was applied with 12 Å cutoff for the Lennard-Jones and screened real-space electrostatic interactions.

The most reasonable structure was then extracted and optimized using two-level ONIOM method[17] as implemented in Gaussian09[18] with a low layer consisting of the DNA template and a high layer with the four dye molecules. The semiempirical PM3 method[19] was used in the low layer, whereas for the high layer, we used the Kohn−Sham formulation of density functional theory (KS-DFT) with ωB97XD functional[20,21] and 6-31+G(d,p) basis set.[22−24] The DNA duplex was kept frozen during optimization and played a role as a template at which the dye molecules were optimized. The final structures shown in Figures 1 and 2 are consistent with the model reported previously by Tomlinson et al.[10] and were used in all further calculations.

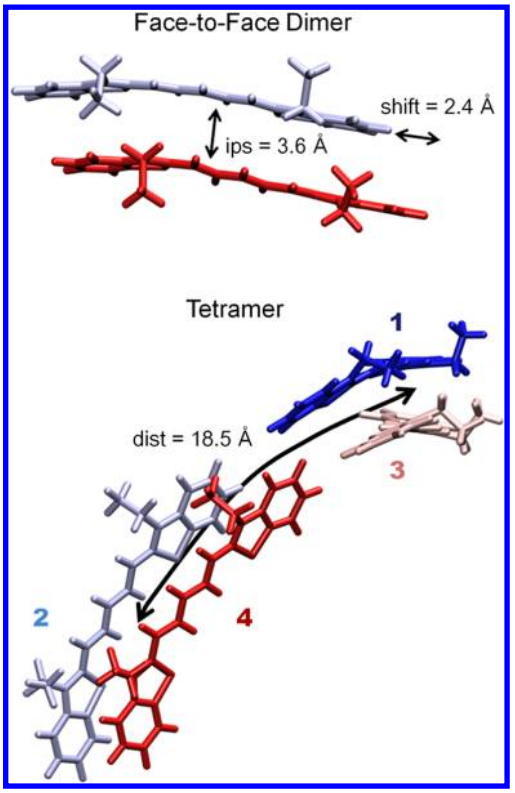

Figure 1. Structural model of four $DiSC_2(5)$ cyanine dyes with the optimized structural parameters. Monomer numbering scheme for the exciton model analysis is also shown. Here, "ips" denotes the interplanar separation distance.

B. Properties of Excited States. The vertical absorption spectra for the studied cyanine dye and their complexes (dimer and tetramer) shown in Figure 1 were computed using the adiabatic time-dependent density functional theory (TD-DFT) with various exchange-correlation functionals, including generalized gradient approximation (GGA) BLYP, hybrid B3LYP and PBE0, the long-range-corrected LC-BLYP, LC-wPBE, and CAM-B3LYP as well as meta-GGA M05-2X and M06-2X.[25−33] All the TD-DFT calculations were carried out using either Gaussian09[18] or Q-CHEM 4.0 packages.[34]

The Pople's 6-31+G(d,p) basis set was used consistently in all the calculations. However, in order to estimate the basis set extension effects, we also performed calculations of the vertical spectra of monomer and dimer using the larger 6-311++G(2df,2pd) basis set.[24,35,36] The solvatochromic effects were studied using the polarizable continuum model of water solvent in the integral equation formalism (IEF-PCM),[37−39] whereas the influence of the DNA template on the calculated CD spectra was investigated using the two-layer ONIOM approach also combined with the IEF-PCM solvation model.

It is generally known that DFT calculations depend, often strongly, on the choice of exchange-correlation functional. This is particularly true for the excitation energies of charge transfer states, such as the bright state of the studied cyanine dye. According to benchmarks, PBE0 and CAM-B3LYP very often outperform other hybrids with the latter being particularly well suited for delocalized excited states as those studied here.[40,41] Moreover, a recently reported study on excitation energies of cyanine dyes shows a very high accuracy of Minnesota functionals (M05 through M08-SO).[42,43] Nevertheless, most of these studies focus on vertical excitation spectra of isolated

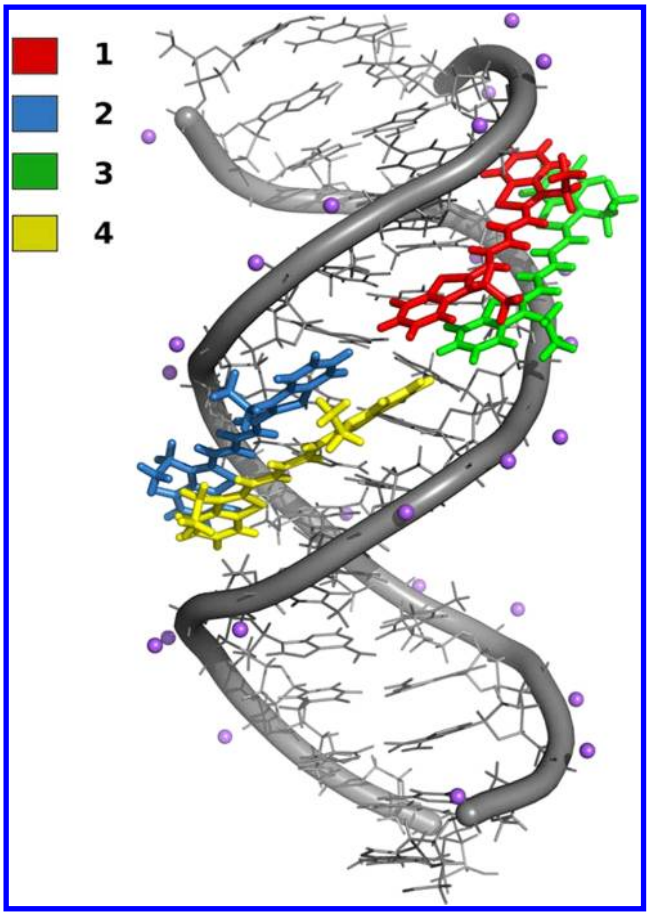

Figure 2. Structural model of four $DiSC_2(5)$ cyanine dyes bound to the minor groove of the AT-10 DNA duplex. The color codes represent the numbering scheme used in the calculations of the exciton coupling energies.

molecules, whereas systematic studies of coupled chromophores that are particularly prone to the so-called self-interaction error are still scarce.[23,27,30,42] In our study, besides the excitation energies, we investigate the performance of selected density functionals also in terms of other spectroscopic properties like the intensities and the excitonic splitting of the electronic absorption bands of molecular aggregates. The calculated excitation energies and the corresponding transition charge densities and transition density moments of an isolated dye molecule were then used in subsequent calculations using the matrix method (described in the following section) to estimate the induced absorption and CD spectra of their complexes.

C. Electronic Couplings and Induced CD. The Frenkel exciton model[44] adopted in this study has been found to be particularly useful for calculating absorption and CD spectra of excitonically coupled multichromophore systems.[45,46] In this approach, the total Hamiltonian $\hat{H}$ of N coupled chromophores (molecules) is partitioned into its molecular contributions $\hat{H}_i$ and the intermolecular Coulomb interaction term $\hat{V}$:

$$\hat{H} = \sum_{i=1}^{N} \hat{H}_i + \hat{V} \tag{1}$$

where $\hat{V}$ is defined in terms of molecular charge density operator $\hat{\rho}_i(\mathbf{r})$ as follows

$$\hat{V} = \frac{1}{2}\sum_{i}^{N}\sum_{j\neq i}^{N}\int d\mathbf{r}_1 \int d\mathbf{r}_2 \frac{\hat{\rho}_i(\mathbf{r}_1)\hat{\rho}_j(\mathbf{r}_2)}{r_{12}} \tag{2}$$

The electronic states of the aggregate are expanded in terms of the molecular adiabatic electronic states ψ_n^i defined as the eigenstates of $\hat{H}_i$ with corresponding eigenvalue E_n^i. In the present study, we treat each chromophore as a two-level system $(n = g,e)$ and, furthermore, take into account only the ground and singly excited states of the aggregate, obtaining the basis states of the form $|\varphi_0\rangle = |\psi_g^1 ... \psi_g^N\rangle$ and $|\varphi_i\rangle = |\psi_g^1 ... \psi_g^{i-1}\psi_e^i\psi_g^{i+1} ... \psi_g^N\rangle$ $(1 \le i \le N)$. In this notation, positive index i is used to denote both the individual molecular site and the corresponding singly excited state, while the ground state is represented by $i = 0$. In these $N + 1$ basis states, the molecular Hamiltonian matrix is diagonal

$$\langle\varphi_i|\sum_{k=1}^{N}\hat{H}_k|\varphi_j\rangle = \begin{cases} \delta_{i0}\sum_{k=1}^{N} E_g^{\,k} + (1-\delta_{i0})[E_g^{\,i} + \sum_{k\neq i}^{N} E_g^{\,k}] & (i = j) \\ 0 & (i \neq j) \end{cases} \tag{3}$$

but the intermolecular coupling is more complicated

$$V_{ij} = \langle\varphi_i|\hat{V}|\varphi_j\rangle = \int d\mathbf{r}_1 \int d\mathbf{r}_2 \frac{S_{ij}(\mathbf{r}_1, \mathbf{r}_2)}{r_{12}} \tag{4}$$

$$S_{ij}(\mathbf{r}_1, \mathbf{r}_2) = \begin{cases} \frac{1}{2}\sum_{p}^{N}\sum_{q\neq p}^{N}\rho_p^{gg}(\mathbf{r}_1)\rho_q^{gg}(\mathbf{r}_2) & (i = j = 0) \\ \rho_i^{eg}(\mathbf{r}_1)\sum_{p\neq i}^{N}\rho_p^{gg}(\mathbf{r}_2) & (i \neq 0; j = 0) \\ \sum_{p\neq i}^{N}\left[\rho_i^{ee}(\mathbf{r}_1)\rho_p^{gg}(\mathbf{r}_2) + \frac{1}{2}\sum_{q\neq i,p}^{N}\rho_p^{gg}(\mathbf{r}_1)\rho_q^{gg}(\mathbf{r}_2)\right] & (i = j; i, j \neq 0) \\ \rho_i^{eg}(\mathbf{r}_1)\rho_j^{ge}(\mathbf{r}_2) & (i \neq j; i, j \neq 0) \end{cases} \tag{5}$$

where $\rho_i^{mn}(\mathbf{r}) = \langle\psi_m^i|\hat{\rho}_i(\mathbf{r})|\psi_n^i\rangle$ denotes the charge density of molecule i in a stationary state $(m = n)$ or the transition charge density $(m \neq n)$ such that

$$\rho_i^{mn}(\mathbf{r}) = N_e\int d\mathbf{r}_2 \int d\mathbf{r}_3 ... \int d\mathbf{r}_{N_e}\psi_m^{i*}(\mathbf{r}, \mathbf{r}_2, \mathbf{r}_3, ..., \mathbf{r}_{N_e})\psi_n^i(\mathbf{r}, \mathbf{r}_2, \mathbf{r}_3, ..., \mathbf{r}_{N_e}) \tag{6}$$

The diagonal terms V_{ii} above are simply the classical intermolecular Coulombic interaction of the aggregate when all molecules are in the ground state $(i = 0)$ or when one of them is in the excited state $(i \neq 0)$. However, the off-diagonal elements V_{ij} $(i \neq j)$ involve the transition charge density and are responsible for mixing of the basis states due to Coulombic interactions.

In principle, we can evaluate all the Coulombic integrals in eq 4 using the charge distributions obtained from electronic structure calculations on a monomer together with the geometric arrangement of the aggregate. However, in the present study, we take a simpler and more conventional approach by ignoring the coupling between the ground state φ_0 and the one-exciton states φ_i $(1 \le i \le N)$. This approximation

dx.doi.org/10.1021/jp309807y | J. Phys. Chem. A 2013, 117, 5909−5918

has been employed in many existing exciton model studies[45−48] and is justified by the large energetic separation of the one-exciton manifold from the ground state. Once this approximation is made, the diagonal terms V_{ii} also become of minor significance and will therefore be ignored. Finally, we obtain the delocalized eigenstates and energies of the aggregate system in the one-exciton space by diagonalizing the following simplified Hamiltonian

$$H_{ij} = \delta_{ij}\Delta E_i + (1 - \delta_{ij})V_{ij} \quad (1 \le i, j \le N) \tag{7}$$

where ΔE_i is the vertical excitation energy of monomer i, and V_{ij} is given by eqs 4 and 5. Computational methods to obtain the exciton coupling V_{ij} are discussed below.

The intensities of the absorption and CD spectra are determined by the oscillator strength f and the rotatory strength R, respectively, of the chromophore. For a 0 → K transition, they are given as[48,49]

$$\begin{aligned} f_{0K} &= \frac{2m_e}{3\hbar^2}(E_K - E_0)|\mu_{0K}|^2 \\ R^L_{0K} &= \mathrm{Im}[\langle 0|\hat{\mu}|K\rangle\cdot\langle K|\hat{m}|0\rangle] \\ R^V_{0K} &= \frac{e\hbar^2}{(E_K - E_0)m_e}\mathrm{Im}[\langle 0|\nabla|K\rangle\cdot\langle K|\hat{m}|0\rangle] \end{aligned} \tag{8}$$

where $\hat{\mu}$ and $\hat{m}$ are electric and magnetic dipole operators, respectively, e is the elementary charge, and m_e is the electron mass. Although the two forms of the rotatory strength, R^L_{0K} and R^V_{0K}, are formally equivalent, the velocity form R^V_{0K} is often preferable because it is origin independent even with approximate wave functions.[50] In the present exciton model, the oscillator/rotatory strength of the aggregate can be constructed from the eigenvalues E_K and eigenvectors $\{U_{lK}\}$ of the exciton Hamiltonian in eq 7. The electric, magnetic, and velocity transition dipole moments are given by $(a = \hat{\mu},\hat{m},\nabla)$

$$\langle K|\hat{a}|0\rangle = \sum_{i=1}^{N} U^*_{iK}\langle\varphi_i|\hat{a}|\varphi_0\rangle = \sum_{i=1}^{N} U^*_{iK}a^i_{eg} \tag{9}$$

where a^i_{eg} is the transition moment of monomer i. Here, it should be emphasized that, unlike the previous exciton models, a^i_{eg} are not identical for different monomers because each monomer has different internal geometry in the aggregate. Then, the oscillator/rotatory strength of the aggregate is obtained from these transition moments and energy eigenvalues E_K using eq 8.

To successfully apply the matrix method described above, one needs to obtain both the monomer excitation energies ΔE_i and the off-diagonal coupling terms V_{ij} that enter the Hamiltonian in eq 7. From eqs 4 and 5, the electrostatic coupling V_{ij} has the form

$$V_{ij} = \int d\mathbf{r}_1 \int d\mathbf{r}_2 \frac{\rho^{eg}_i(\mathbf{r}_1)\rho^{ge}_j(\mathbf{r}_2)}{r_{12}} \tag{10}$$

with the transition charge density $\rho^{eg}_i(\mathbf{r})$ given by eq 6. These equations, however, are not easily tractable, and for this reason, many approximate methods have been proposed ,which come down to introduction of a certain approximate representation of the transition charge densities.

The most simplified point dipole approximation (PDA) is derived from the leading term of the multipole expansion of the coupling term V_{ij}, which is expressed in terms of two interacting point transition dipoles. However, it has been shown that the PDA approach provides inaccurate description for intermolecular distances smaller than 20 Å.[51] For this reason, we have found PDA not suitable for our purposes and decided to focus on the more reliable methods.

One of the methods that has provided a better description of the transition density is the transition charge from electrostatic potential (TrESP).[51] In this method, the Coulombic interaction is calculated between atomic partial charges obtained by least-squares fitting to the electrostatic potential $\varphi(\mathbf{r})$ derived from the transition densities. Such electrostatic potential at point $\mathbf{r}$ is given in terms of the transition density matrix $P^{eg}_{\mu\nu}$ of a monomer in atomic orbital (AO) basis $\{\phi_\mu\}$ by

$$\varphi(\mathbf{r}) = \sum_{\mu,\nu} P^{eg}_{\mu\nu}\int d\mathbf{r}'\phi^*_\mu(\mathbf{r}')\phi_\nu(\mathbf{r}')/|\mathbf{r} - \mathbf{r}'| \tag{11}$$

The TrESP method has been found to give much more reliable results than simple PDA, and it was shown that the problems related to short distance limitations are partially overcome in this approach.[51] The electrostatic potential for TrESP method was calculated in this work on a previously generated grid of randomly sampled points consisting of 2500 points per atom. The fitting of atomic partial charges was done using CHELPBOW program.[52] The charges on hydrogen atoms were summed into those of heavy atoms.

An interesting attempt to overcome the limitations of PDA approximation while keeping the feasibility of the approximate electrostatic treatment was the transition density cube (TDC) method proposed by Krueger, Scholes, and Fleming.[53] In this method, the Coulombic couplings of the transition densities for two interacting moieties are calculated from the transition density cubes (TDCs), i.e., the discrete representation of these densities on a cubic grid. Such a representation can be routinely obtained from various ab initio packages including Gaussian09 and Q-CHEM 4.0 used in this study. Although this method combines an even more realistic representation of the shapes of the transition densities and can be used also at relatively short intermolecular separations, it has some drawbacks. One of the limitations is a certain deterioration of the results in the case of substantial overlap of the transition densities of interacting species and hence their discrete representation.[46] Nonetheless, it provides a relatively simple approach of substantially improved performance in comparison to the PDA and TrESP approximations. The transition density cubes used for the calculation of the electronic couplings were generated using the Q-CHEM package with a typical dimension of 27 × 22 × 14 Å^3 and assuming various grid densities ranging from 0.008 to 0.037 Å^3 per element. The electronic couplings were then calculated using the TDC software package developed by Krueger et al.[53]

In principle, the most accurate estimations of excitonic couplings reported in this work are those obtained using the fragment-excitation difference (FED) method,[54] which belongs to the so-called eigenstate-based methods and has been implemented recently in the Q-CHEM quantum chemistry package. In this method, the diabatic donor (D) and acceptor (A) states are assumed to be a linear combination of the eigenstates under the two-state approximation. For a pair of singly excited states i and j, the excitonic coupling can be estimated as

$$V_{ij} = \frac{(E_i - E_j)|\Delta x_{ij}|}{\sqrt{(\Delta x_{ii} - \Delta x_{jj})^2 + 4\Delta x^2_{ij}}} \tag{12}$$

dx.doi.org/10.1021/jp309807y | J. Phys. Chem. A 2013, 117, 5909−5918

where Δx_{ij} is the difference in the excitation charge densities used to find localized states

$$\Delta x_{ij} = \int_{\mathbf{r}\in D} \rho^{ij}(\mathbf{r})\mathrm{d}\mathbf{r} - \int_{\mathbf{r}\in A} \rho^{ij}(\mathbf{r})\mathrm{d}\mathbf{r} \quad (13)$$

One should note, however, that in practice the charge densities in the above equation are approximated with Mulliken population analysis, and hence the calculated coupling constants may be biased and inaccurate (particularly at short intermolecular distances). At a large separation, both FED and Coulomb couplings become identical and have the same asymptotic dipole−dipole (r^{-3}) decay. In the following section, the coupling constants obtained with these three different methods are used to describe the electronic excited states of the dye aggregates and their CD and ORD properties within the exciton model framework.

III. RESULTS AND DISCUSSION

A. Optimized Aggregate Structure. The model of the H-type aggregated $DiSC_2(5)$ that was previously reported by Tomlinson et al.[10] was found to be particularly helpful in the present attempt to prepare the initial structure for MD simulation. However, it is worth mentioning that, despite several notable studies on this or similar systems,[1,2,10,55−58] there has been no attempt to obtain the structure of the aggregate using ab initio/DFT methods. The MD simulation study was performed as described in the previous section. In this process, the initial, nearly linear pair of dimers with a minimal offset applied to avoid steric clashes between the monomeric dyes resulted in a helically twisted structure with a shift characteristic for H-type assemblies (where two monomers in the face-to-face dimer are shifted from each other by less than 8 Å). According to the MD trajectories, the molecular structure seems to be more stable when the offset between the monomers is larger than 2 Å. These findings are consistent with the results of Tomlinson et al.[10] Nevertheless, in order to obtain an accurate model that could be used for reproducing the experimental CD and ORD spectra, further quantum chemistry optimizations of the coupled chromophore system had to be carried out. The ONIOM approach has been proven to be a very reasonable choice in the case of the large system containing distinguishable reaction centers.[17] In the present study, the dye tetramer was treated using the hybrid ωB97XD functional, which includes both long-range and empirical dispersion corrections and thus provides a good description of the noncovalent interactions between the dye molecules and the base pairs in the DNA minor groove. The DNA itself was kept frozen during the optimization and was treated at the PM3 level of theory, which we found quite suitable and quickly converging even for the present DNA structure consisting of more than 800 atoms. The optimized aggregate structure is shown in Figure 1, and it can be directly compared with the previous models in terms of the three structural parameters introduced by Tomlinson et al.:[10] shift, interplanar separation (ips), and the distance between the centers of mass of the face-to-face dimers. Thus, the obtained results are fairly consistent with the previous estimation and are summarized in Figure 1.

B. Excited State Calculations. There has been a growing interest in the spectra of cyanine dyes due to a wide range of potential applications including artificial light harvesting[59] and fluorescent labeling of biomolecules.[60] Consequently, a number of attempts have been made to reproduce the experimental spectra of these compounds. Quite a few studies among them employed the TD-DFT method.[40,43,61,62] More reliable CASSCF/CASPT2 results have also been reported.[63,64] However, the size of the system for which these methods can be applied is still rather limited. Specifically, for computational feasibility, the active space is often chosen to be smaller than the actual π-electronic space, which could greatly reduce the reliability of results. For instance, in the case of $DiSC_2(5)$ that contains aromatic rings on each side of a polymethine bridge, the limitations of the active space would likely result in very unreasonable excitation energies and transition strengths. Thus, considering the moderate computational cost and reasonable accuracy, for the time being, TD-DFT is still the method of choice. In the present study, we applied the TD-DFT method with a broad selection of exchange-correlation functionals to investigate UV−vis absorption, CD, and ORD spectra of the cyanine dye aggregates consisting of two and four molecules. The TD-DFT results obtained for isolated dye molecules were also used to parametrize the excitonic Hamiltonian in the matrix method.

The excitation energies and transition strengths obtained using various methods for a single $DiSC_2(5)$ molecule both in the gas-phase and in IEF-PCM model of water solvent are summarized in Table 1 and compared against the experimental estimates. They indicate that, although TD-DFT generally overestimates the excitation energies by 50−100 nm, the calculated bathochromic solvatochromic shifts are of the same order (about 40 nm), and the observed discrepancies may come partially from inadequacies of the approximate representation of solvent in the PCM model. The basis set extension does not improve the agreement significantly either for monomer or dimer, which means that the 6-31+G(d,p) basis set should provide reliable results also for tetramer. It should be noted that the oscillator strengths predicted by all the functionals are very close to the experimentally estimated

Table 1. Excitation Energies (ΔE) Oscillator Strengths (f) of the Most Intense Lowest-Lying Excited State of $DiSC_2(5)$ Dye Estimated Using Various DFT Functionals and 6-311++G(2df,2pd) Basis Set; the Results in Parentheses Were Estimated Using Smaller 6-31+G(d,p) Basis Set; the PCM Results Were Obtained with the IEF-PCM Model for Water Solvent

functional	ΔE (nm)		Y	
	Vacuum			
BLYP	553	(549)	1.94	(1.97)
B3LYP	530	(527)	2.05	(2.07)
CAM-B3LYP	522	(520)	2.10	(2.11)
PBE0	522	(520)	2.10	(2.12)
LC-ωPBEh	522	(518)	1.91	(1.92)
M05-2X	519	(518)	2.10	(2.11)
M06-2X	527	(526)	2.08	(2.09)
	PCM			
BLYP	593	(589)	2.12	(2.14)
B3LYP	569	(566)	2.20	(2.07)
CAM-B3LYP	561	(592)	2.22	(2.11)
PBE0	561	(558)	2.24	(2.25)
LC-ωPBEh	566	(566)	2.24	(2.23)
M05-2X	558	(558)	2.22	(2.23)
M06-2X	568	(568)	2.21	(2.21)
exptl[a]	646		1.74	

[a]Experimental results taken from ref 1.

dx.doi.org/10.1021/jp309807y | J. Phys. Chem. A 2013, 117, 5909−5918

values, which indicates reliability of the corresponding transition densities and hence the coupling constants calculated based on these densities.

The spectral properties of dimeric forms of $DiSC_2(5)$ are presented in Table 2, which also displays the emergence of the

Table 2. Excitation Energies (nm) of Major Components of the CD Spectrum (λ^+ and λ^-) of the Face-to-Face and End-to-End Dimeric Forms of $DiSC_2(5)$ Aggregate Calculated at the TD-DFT Level in Vacuum Using Various Functionals and 6-31+G(d,p) Basis Set; Rotatory Strengths Calculated in Velocity Formulation Are Given in Parentheses in 10^{-40} cgs Units

functional	λ_1^+	f^+	λ_1^-	f^-
Face-to-Face Dimer (1−3)				
B3LYP	653 (−22)	0.00	492 (237)	3.01
CAM-B3LYP	632 (−94)	0.00	473 (213)	3.35
PBE0	622 (−25)	0.00	482 (234)	3.17
LC-ωPBEh	601(−101)	0.00	463 (201)	3.61
M05-2X	639 (−79)	0.00	471 (206)	3.35
M06-2X	655 (−77)	0.00	479 (195)	3.27
End-to-End Dimer (1−2)				
B3LYP	540 (2138)	2.15	513 (−2174)	1.74
CAM-B3LYP	526 (1520)	2.19	492 (−1583)	1.88
PBE0	531 (2068)	2.19	504 (−2115)	1.79
LC-ωPBEh	565 (503)	2.25	505 (−616)	1.92
M05-2X	525 (1664)	2.20	492 (−1734)	1.87
M06-2X	533 (1694)	2.18	500 (−1770)	1.85

CD spectrum upon formation of the complex. Here, we extracted two molecular structures from the previously optimized aggregate, i.e., the face-to-face and end-to-end dimers, and carried out TD-DFT calculations. In both cases, the strong splitting of the energy levels can be observed. In the case of the face-to-face dimer, the higher energy transition carries most of the intensity in the absorption spectrum as can be deduced from the exciton model analysis for the H-type aggregate.[1,65] However, as expected, the face-to-face dimer does not exhibit significant CD or ORD spectra. However, the end-to-end dimer resembles the helical structure of the DNA, and because of its oblique geometry, the TD-DFT calculation predicts two allowed transitions and a strong CD signal. The intensity is shared nearly equally between the two states, and the positive Cotton effect is observed, which already resembles the major couplet feature of the experimentally measured CD spectrum (blue line) of the tetrameric aggregate in Figure 3.

The most elaborate calculations were done for the tetrameric dye aggregate, and the resulting CD peak positions and amplitudes are summarized in Table 3. It shows that all TD-DFT estimates are rather similar to one another in the splitting energy or $\Delta\bar{\lambda}$ (= $\lambda^+ - \lambda^-$) that ranges from 23 to 32 nm in vacuum, close to the experimental estimates of 17−19 nm. The previously proposed exciton coupling model predicts the presence of four levels among which two correspond to higher energy states and are responsible for the intense CD signal.[1,10,57] Our TD-DFT calculations and analysis of the experimental data show that the actual spectral features are more complicated in nature. In addition to the doublet states with large rotatory strengths, in most cases, we observe six nearby states with smaller rotatory strengths. Interestingly, the experimental CD spectra of $DiSC_2(5)$ oligomer exhibit a small positive peak at about 670 nm whose origin had not been

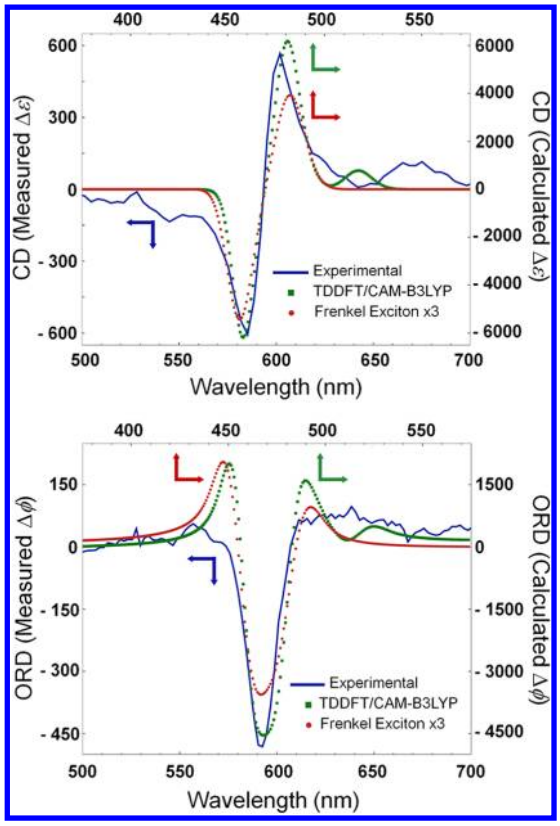

Figure 3. CD (top) and ORD (bottom) spectra of the tetrameric cyanine-dye aggregate. The spectra from the gas-phase TD-DFT/CAM-B3LYP calculation (green dots) and the exciton model (red dots) are displayed on the scale of top and right axes, while the experimental spectrum (blue line) is drawn in reference to the bottom and left axes (see colored arrows for guide). In the exciton model case, the TDC approach at the B3LYP/6-311++G(2df,2pd) level was used to calculate the electronic coupling constants. A Gaussian line shape with the full width at half-maximum of 0.11 eV was assumed for all the transition bands.

Table 3. Excitation Energies (nm) of the Major Components of the CD Spectrum (λ_1^+ and λ_1^-) of a Tetrameric $DiSC_2(5)$ Aggregate Calculated at the TD-DFT Level in the Gas Phase Using Various Functionals and 6-31+G(d,p) Basis Set; the Position and Intensity of the Additional Small Positive Peak Is Given in the Column Labeled λ_2^+. Rotatory Strengths Calculated by Using the Origin-Independent Velocity Formulation Theory Are Given in Parentheses in 10^{-40} cgs Units

functional	λ_1^-	λ_1^+	λ_2^+	$\Delta\bar{\lambda}$
B3LYP	478 (−3214)	506 (4856)		29
CAM-B3LYP	458 (−4054)	490 (4011)	517 (564)	32
PBE0	469 (−3588)	497 (4820)		28
LC-ωPBEh	451 (−2702)	484 (4071)		33
M05-2X	458 (−4325)	481 (4232)	520 (608)	23
M06-2X	467 (−3453)	490 (5153)	532 (510)	24
exptl[a]	588	607	∼670	19
exptl[b]	585	602		17

[a]Ref 1. [b]Ref 3.

studied before. This peak shows up in the AT-10 template and becomes even more intense in $[poly(dA\text{-}dT)]_2$ (a DNA copolymer with alternating bases A and T in each strand) template. This peak is reproduced by our TD-DFT calculations

dx.doi.org/10.1021/jp309807y | J. Phys. Chem. A 2013, 117, 5909−5918

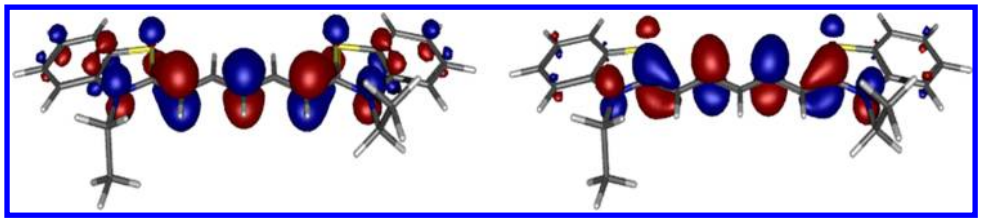

Figure 4. HOMO (H) and LUMO (L) orbitals of monomeric $DiSC_2(5)$ dye, respectively.

on tetramer and it is denoted as λ_2^+ in Table 3. As can be seen in Figure 3, its intensity is about an order of magnitude smaller than that of the major peak. This suggests that this side peak is intrinsically related to the aggregate structure and does not originate from either solvent effects or the presence of the DNA template. In order to elucidate the origin of this spectral feature, we analyzed the calculated TD-DFT spectra in terms of relevant molecular orbitals. In the case of a single dye molecule, the UV−vis spectrum is dominated by a single intense transition corresponding essentially to the HOMO−LUMO excitation (Figure 4). In the face-to-face dimer, these orbitals localized on monomers 1 and 2 give rise to four orbitals being their linear combination (given from lowest to highest energy): $H_1 + H_2$; $H_1 - H_2$; $L_1 + L_2$; $L_1 - L_2$.

There are also four transitions involved that are shown schematically in the diagram in Figure 5. Since the interactions

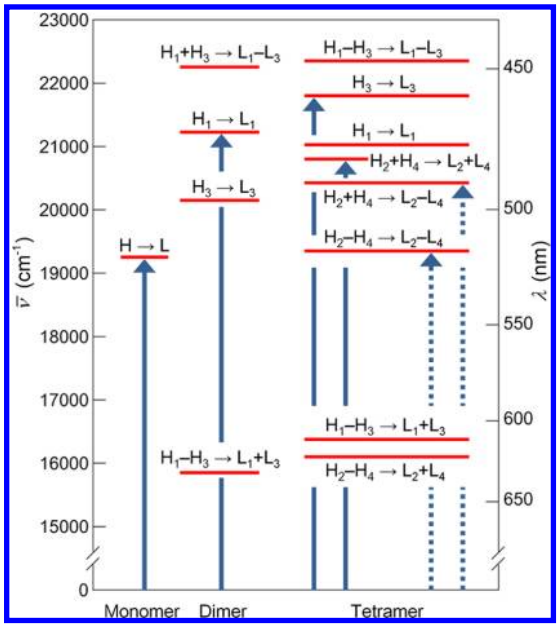

Figure 5. Schematic diagram of selected excited states of monomer, face-to-face dimer, and tetramer resulting from TD-DFT/CAM-B3LYP calculations. Bright states with large oscillator strengths are indicated with solid arrows and those less intensive transitions ($f < 1$) with dashed arrows. The remaining transitions are forbidden. H_i and L_i represent approximately the HOMO and LUMO orbitals of monomer i.

among two H-dimers in tetramer are relatively weak, the corresponding orbitals form a set of four doubly degenerate orbitals that are involved in eight excited states (Figure 5). Considering the above orbital analysis, we believe that the additional peak observed in the experimental CD spectrum is associated with a weak transition to one of the lower energy states, i.e., $H_2 + H_4 \rightarrow L_2 - L_4$ transition (Figure 5), which is formally forbidden in an ideal H-type aggregate. Thus, this additional peak appears to be yet another manifestation of the induced CD effect arising from the end-to-end interaction of two H-type dimeric units.

Similar calculations were also carried out for the tetrameric dye with the IEF-PCM solvation model, two-layer ONIOM, and the combination of the two in order to investigate the influence of the water solvent and the presence of the DNA template on the calculated absorption, CD and ORD spectra. The obtained results are not appreciably different from the gas phase data shown above and thus are not presented here. This indicates that the influence of the DNA template or continuum solvent on the electronic spectra is rather small.

C. Exciton Coupling Model. The exciton coupling model has been extensively used for the calculation of absorption, CD, ORD, and two-dimensional electronic spectra of light-harvesting systems,[46,66−68] coupled porphyrin aggregates,[69] and many other coupled organic molecules.[70,71] The success of this method hinges on the realistic description of the distance-dependent couplings among interacting chromophores. As mentioned before, if the interchromophore distance becomes considerably small, more sophisticated methods beyond the transition dipole approximation have to be used. In our study, we deal with dimers whose interplanar separation of 3.60 Å causes a significant overlap of their transition densities. Thus, the calculation of the electronic coupling of a face-to-face dimer becomes a nontrivial task. We take the values of 3500 cm^{-1} for $2\beta_H$ and 330 cm^{-1} for $2\gamma_H$ evaluated from 77 K absorption spectra by Peteanu and co-workers[57] as reference and carry out a comparative study using TrESP, TDC, and FED approaches. Here, $2\beta_H$ is the primary splitting of the excited states in the face-to-face dimer, and $2\gamma_H$ represents the secondary splitting in the tetramer with respect to the states of the face-to-face dimer. The value of the secondary splitting constant γ_H has previously been treated as the magnitude of the end-to-end coupling energy.[57] However, it should be noted that, due to the shift between the dye molecules in the face-to-face dimer in Figure 1, we needed to consider two end-to-end and two cross-couplings that could be substantially different in magnitude. The results are summarized in Table 4. First, the coupling constant V_{13} for two monomers in the face-to-face configuration is calculated as ∼1600 cm^{-1} with the TrESP method, and it can be up to 1000 cm^{-1} larger with the TDC and FED methods. There values are in reasonable agreement with the aforementioned experimental estimate of β_H (1750 cm^{-1}). Second, the calculated coupling constants V_{12} and V_{34} for the end-to-end interaction are much smaller than V_{13}, and they are of similar magnitude as the experimental estimate of γ_H (165 cm^{-1}). In addition, it can be seen that the two cross-coupling terms V_{14} and V_{23} are indeed quite different, and the former is up to three times larger than the latter due to the shift in the dimer configuration. In general, all the calculation methods used here give quite consistent results for all the pairs.

dx.doi.org/10.1021/jp309807y | J. Phys. Chem. A 2013, 117, 5909−5918

Table 4. Coupling Constants in cm^{-1} Evaluated Using TDC, TrESP, and FED Methods ($V_{13} = V_{24}$) Based on the Transition Densities Obtained from TD-DFT Calculations Using the Selected Functionals and 6-311++G(2df,2pd) Basis Set; the Corresponding Estimates Obtained Using the Smaller 6-31+G(d,p) Basis Set Are Given in Parentheses

	BLYP	B3LYP	LC-ωPBEh
		TrESP	
V_{12}	307 (310)	322 (324)	324 (324)
V_{13}	1586 (1489)	1561 (1574)	1594 (1591)
V_{14}	445 (446)	463 (467)	468 (470)
V_{23}	172 (161)	167 (167)	168 (167)
V_{34}	307 (285)	295 (296)	297 (298)
		TDC[a]	
V_{12}	162 (162)	322 (183)	168 (167)
V_{13}	1998 (1998)	2186 (2144)	1891 (1907)
V_{14}	203 (203)	414 (488)	467 (469)
V_{23}	188 (192)	197 (126)	124 (123)
V_{34}	316 (282)	293 (287)	320 (319)
		FED	
V_{12}	(502)	(374)	(342)
V_{13}	(1378)	(1231)	(2602)
V_{14}	(526)	(460)	(458)
V_{23}	(225)	(173)	(186)
V_{34}	(329)	(308)	(304)

[a]The volume of 0.008 A^3 was applied for a single cube element.

Nevertheless, it is well-known that the TDC method depends strongly on the size of the cubic grid. Our study indicates that, to obtain numerically consistent results, the size of the volume element should be smaller than 0.008 $Å^3$. With a proper choice of the grid size, the TDC method appears to perform very well for systems in which the interacting states can be easily identified, e.g., coupled multichromophore systems like J- or H-aggregates and light-harvesting complex proteins.

D. Simulated CD and ORD Spectra. Once all the parameters are determined, it becomes ready to numerically simulate the CD and ORD spectra for the sake of comparison with the experimental results. The CD and ORD spectra are determined by the difference of the optical activity susceptibility $\chi_{L/R}(\omega)$ to the left- and right-circularly polarized lights. Assuming a Gaussian line shape with width Ω_{0K} for the $0 \rightarrow K$ band, the complex chiral susceptibility is given by[72]

$$\Delta\chi(\omega) = \chi_L(\omega) - \chi_R(\omega) = \sum_K \frac{2\sqrt{\pi}\,i}{3\hbar\Omega_{0K}} R_{0K} \times \left[e^{-(\omega-\omega_{K0})^2/2\Omega_{0K}^2} \mathrm{erfc}\left(-i\frac{\omega-\omega_{K0}}{\sqrt{2}\,\Omega_{0K}}\right) + e^{-(\omega+\omega_{K0})^2/2\Omega_{0K}^2} \mathrm{erfc}\left(-i\frac{\omega+\omega_{K0}}{\sqrt{2}\,\Omega_{0K}}\right)\right] \quad (14)$$

where ω_{K0} is the average transition frequency of the $0 \rightarrow K$ band and erfc represents the complementary error function. The real and imaginary part of $\Delta\chi(\omega)$ are directly related to the amplitude of the ORD and CD signals, respectively, and in principle, they can be converted from each other by the Kramers–Kronig transformation. The numerically calculated CD spectra in Figure 3 were obtained by convoluting the calculated rotatory strengths in velocity form with Gaussian curves of constant width using the imaginary part of eq 12. The ORD spectra are the numerical Kramers–Kronig transforms of the corresponding CD spectra.[73] Unfortunately, the experimental spectra of coupled systems happen to be quite difficult to deconvolute, and the absolute magnitudes of calculated rotatory strengths are very often overestimated. We have found it the easiest and the most reasonable to use the half bandwidth as a fitting parameter that is chosen for the best resemblance with the experimental curve. The best fit for our TD-DFT results was obtained when the full width at half-maximum was equal to 0.11 eV. We found that the experimental energy gap between the two major peaks is smaller than our TD-DFT estimate so that, for the sake of comparison, the wavelength for TD-DFT spectra is shown on the top axis of each panel in Figure 3. In the case of the spectra obtained using the exciton model, the monomer transition energies were taken from the TD-DFT calculations so that one can directly compare the exciton-model-based spectra with the TD-DFT ones. Note that the evaluated transition energies of the coupled multichromophore system depend mainly on the accuracy of the calculated Coulombic interaction terms and on the amount of information that is lost due to assumption that the interaction between the monomers is purely electrostatic. The latter seems to make a significant influence on the relative magnitudes of rotatory strength. Nevertheless, it was found that the matrix method is capable of reproducing the main features of the CD spectrum, and together with the methods used in this study to evaluate interchromophore interactions, it can be successfully applied for efficient calculations of CD/ORD spectra of even more complicated molecular systems.

IV. SUMMARY

In this article, we have studied the circular dichroism of self-assembled aggregates of the cyanine dye $DiSC_2(5)$ that exhibit characteristic induced chirality when templated into the minor groove of DNA double helices. TD-DFT calculations on the monomeric form of the compound show that the lowest HOMO–LUMO type excitation carries a large oscillator strength and corresponds to the main peak of the UV–vis absorption spectrum. In a dimer, the calculated spectral feature depends critically on the intermolecular arrangement. When two monomers are facing each other with large contact (face-to-face dimer) as in an H-aggregate, the transition is allowed only to the higher state among the two, resulting in a blue shift of the spectral band. However, in an end-to-end arrangement, transitions to both of the levels become allowed with comparable oscillator strengths. Also, the end-to-end dimer exhibits about an order of magnitude larger rotatory strengths than the face-to-face dimer, due to the helical twist that is substantial only in the former arrangement. When two face-to-face dimers are combined in an end-to-end way, the resulting tetramer exhibits two intense transitions that are fifth and seventh lowest in energy, and they carry large rotatory strengths, about twice that in the end-to-end dimer. Moreover, the tetramer exhibits a weaker transition to the red side of the major doublet that involves the fourth excited state. These results are fully consistent with the experimental absorption and CD/ORD spectra and clearly demonstrate the induced CD effect arising from the right-handed helical twist structure of the dye aggregates. This study also indicates that the CAM-B3LYP functional is best suited for the present system.

We have also investigated the induced CD of the tetramer based on a much simpler exciton coupling model with parameters obtained from the TD-DFT calculations on the

dx.doi.org/10.1021/jp309807y | J. Phys. Chem. A 2013, 117, 5909–5918

monomer and intermolecular Coulombic interactions between monomeric transition charge densities derived from TrESP, TDC, and FED calculations. This exciton model analysis predicted a large CD signal with the positive Cotton effect that clearly reproduces the main doublet feature found in our recent experimental spectra and the present TD-DFT calculation results. Such quantitative agreement testifies the validity of the present computational methods because the intrinsic rotatory strength of a monomeric dye vanishes and a large rotatory strength is attainable only when the transition dipoles reflecting the chiral arrangement of monomers in the aggregate are properly calculated. However, because of the simple nature of a two-level description for the electronic transition of each monomer, the exciton model could not capture the small but important peak that appears at around 670 nm in the experimental CD spectrum. Nonetheless, the success of the exciton coupling theory in reproducing the major coupling pattern in the CD is encouraging because it opens up the possibility to study CD of even larger-scale aggregates of dye molecules as well as their association−dissociation dynamics. For the present $DiSC_2(5)$ dye, we found that the TD-DFT calculation of a tetramer takes well over an order of magnitude longer time than that of a monomer. Thus, direct application of the TD-DFT method to larger systems would quickly become impractical. In this regard, we expect that the exciton coupling theory, both in the present and potentially more refined forms, could be well suited for the study of induced optical activities of a wide range of dye aggregates and that the outcome of the present article could provide a useful guideline in such studies in the future.

AUTHOR INFORMATION

Corresponding Author

*E-mail: mcho@korea.ac.kr.

Notes

The authors declare no competing financial interest.

ACKNOWLEDGMENTS

This work was supported by NRF (No. 2011-0020033 and 2009-0078897) and KBSI (T32401) grants to M.C. and the National Science Centre grant (No. DEC-2011/03/B/ST4/00587) to R.W.G. Also, the support from the Wroclaw Center for Networking and Supercomputing is gratefully acknowledged. We would like to thank Professor U. Ryde for sending the CHELP-BOW source code and Dr. B. Krueger for generously providing us his TDC calculation package.

REFERENCES

(1) Seifert, J. L.; Connor, R. E.; Kushon, S. A.; Wang, M.; Armitage, B. A. *J. Am. Chem. Soc.* **1999**, *121*, 2987−2995.
(2) Hannah, K. C.; Armitage, B. A. *Acc. Chem. Res.* **2004**, *37*, 845−853.
(3) Eom, I.; Ahn, S.-H.; Rhee, H.; Cho, M. *Opt. Express* **2011**, *19*, 10017−10028.
(4) Rhee, H.; Eom, I.; Ahn, S.-H.; Cho, M. *Chem. Soc. Rev.* **2012**, *41*, 4457−4466.
(5) Rhee, H.; June, Y.-G.; Kim, Z. H.; Jeon, S.-J.; Cho, M. *J. Opt. Soc. Am. B* **2009**, *26*, 1008−1017.
(6) Rhee, H.; June, Y.-G.; Lee, J.-S.; Lee, K.-K.; Ha, J.-H.; Kim, Z. H.; Jeon, S.-J.; Cho, M. *Nature* **2009**, *458*, 310−313.
(7) Eom, I.; Ahn, S.-H.; Rhee, H.; Cho, M. *Phys. Rev. Lett.* **2012**, *108*, 103901.
(8) Rhee, H.; Ha, J.-H.; Jeon, S.-J.; Cho, M. *J. Chem. Phys.* **2008**, *129*, 094507.
(9) Lepetit, L.; Chériaux, G.; Joffre, M. *J. Opt. Soc. Am. B* **1995**, *12*, 2467−2474.
(10) Tomlinson, A.; Frezza, B.; Kofke, M.; Wang, M.; Armitage, B. A.; Yaron, D. *Chem. Phys.* **2006**, *325*, 36−47.
(11) Tomlinson, A.; Yaron, D. *J. Comput. Chem.* **2003**, *24*, 1782−1788.
(12) Bansal, M.; Bhattacharyya, D.; Ravi, B. *Comput. Appl. Biosci.* **1995**, *11*, 281−287.
(13) Case, D. A.; Darden, T. A.; Cheatham, T. E.; Simmerling, C. L.; Wang, J.; Duke, R. E.; Luo, R.; Walker, R. C.; Zhang, W.; Merz, K. M.; et al. *Amber 11*; University of California: San Francisco, CA, 2010.
(14) Wang, J.; Cieplak, P.; Kollman, P. *J. Comput. Chem.* **2000**, *21*, 1049−1074.
(15) Price, D. J.; Brooks, C. L., III. *J. Chem. Phys.* **2004**, *121*, 10096−10103.
(16) Darden, T.; York, D.; Pedersen, L. *J. Chem. Phys.* **1993**, *98*, 10089−10092.
(17) Dapprich, S.; Komáromi, I.; Byun, K. S.; Morokuma, K.; Frisch, M. J. *J. Mol. Struct.* **1999**, *461*−*462*, 1−21.
(18) Frisch, M. J.; Trucks, G. W.; Schlegel, H. B.; Scuseria, G. E.; Robb, M. A.; Cheeseman, J. R.; Scalmani, G.; Barone, V.; Mennucci, B.; Petersson, G. A.; et al. *Gaussian 09*, revision C.01; Gaussian Inc.: Wallingford, CT, 2009.
(19) Stewart, J. J. P. *J. Comput. Chem.* **1989**, *10*, 209−220.
(20) Chai, J.-D.; Head-Gordon, M. *J. Chem. Phys.* **2008**, *128*, 084106.
(21) Chai, J.-D.; Head-Gordon, M. *Phys. Chem. Chem. Phys.* **2008**, *10*, 6615−6620.
(22) Ditchfield, R.; Hehre, W. J.; Pople, J. A. *J. Chem. Phys.* **1971**, *54*, 724−728.
(23) Hehre, W. J.; Ditchfield, R.; Pople, J. A. *J. Chem. Phys.* **1972**, *56*, 2257−2261.
(24) Clark, T.; Chandrasekhar, J.; Spitznagel, G. W.; Schleyer, P. V. R. *J. Comput. Chem.* **1983**, *4*, 294−301.
(25) Becke, A. D. *J. Chem. Phys.* **1993**, *98*, 5648−5652.
(26) Lee, C.; Yang, W.; Parr, R. G. *Phys. Rev. B* **1988**, *37*, 785−789.
(27) Perdew, J. P.; Burke, K.; Ernzerhof, M. *Phys. Rev. Lett.* **1996**, *77*, 3865−3868.
(28) Iikura, H.; Tsuneda, T.; Yanai, T.; Hirao, K. *J. Chem. Phys.* **2001**, *115*, 3540−3544.
(29) Tawada, Y.; Tsuneda, T.; Yanagisawa, S.; Yanai, T.; Hirao, K. *J. Chem. Phys.* **2004**, *120*, 8425−8433.
(30) Vydrov, O. A.; Heyd, J.; Krukau, A. V.; Scuseria, G. E. *J. Chem. Phys.* **2006**, *125*, 074106.
(31) Yanai, T.; Tew, D. P.; Handy, N. C. *Chem. Phys. Lett.* **2004**, *393*, 51−57.
(32) Zhao, Y.; Schultz, N. E.; Truhlar, D. G. *J. Chem. Theory Comput.* **2006**, *2*, 364−382.
(33) Zhao, Y.; Truhlar, D. *Theor. Chem. Acc.* **2008**, *120*, 215−241.
(34) Shao, Y.; Molnar, L. F.; Jung, Y.; Kussmann, J.; Ochsenfeld, C.; Brown, S. T.; Gilbert, A. T. B.; Slipchenko, L. V.; Levchenko, S. V.; O'Neill, D. P.; et al. *Phys. Chem. Chem. Phys.* **2006**, *8*, 3172−3191.
(35) Krishnan, R.; Binkley, J. S.; Seeger, R.; Pople, J. A. *J. Chem. Phys.* **1980**, *72*, 650−654.
(36) Frisch, M. J.; Pople, J. A.; Binkley, J. S. *J. Chem. Phys.* **1984**, *80*, 3265−3269.
(37) Cances, E.; Mennucci, B.; Tomasi, J. *J. Chem. Phys.* **1997**, *107*, 3032−3041.
(38) Scalmani, G.; Frisch, M. J. *J. Chem. Phys.* **2010**, *132*, 114110.
(39) Tomasi, J.; Mennucci, B.; Cammi, R. *Chem. Rev.* **2005**, *105*, 2999−3094.
(40) Jacquemin, D.; Perpete, E. A.; Scuseria, G. E.; Ciofini, I.; Adamo, C. *J. Chem. Theory Comput.* **2008**, *4*, 123−135.
(41) Jacquemin, D.; Perpète, E. A.; Ciofini, I.; Adamo, C. *Acc. Chem. Res.* **2009**, *42*, 326−334.
(42) Jacquemin, D.; Perpète, E. A.; Ciofini, I.; Adamo, C.; Valero, R.; Zhao, Y.; Truhlar, D. G. *J. Chem. Theory Comput.* **2010**, *6*, 2071−2085.
(43) Jacquemin, D.; Zhao, Y.; Valero, R.; Adamo, C.; Ciofini, I.; Truhlar, D. G. *J. Chem. Theory Comput.* **2012**, *8*, 1255−1259.
(44) Frenkel, J. *Phys. Rev.* **1931**, *37*, 1276−1294.

(45) Bayley, P. M.; Nielsen, E. B.; Schellman, J. A. *J. Phys. Chem.* **1969**, *73*, 228−243.
(46) Fujimoto, K. J. *J. Chem. Phys.* **2010**, *133*, 124101.
(47) Ecoffet, C.; Markovitsi, D.; Millié, P.; Lemaistre, J.-P. *Chem. Phys.* **1993**, *177*, 629−643.
(48) *Circular Dichroism: Principles and Applications*; 2nd ed.; Berova, N., Nakanishi, K., Woody, R. W., Eds.; Wiley-VCH: New York, 2000.
(49) Atkins, P. W. *Molecular Quantum Mechanics*, 2nd ed.; Oxford University Press: Oxford, U.K., 1983.
(50) Moffitt, W. *J. Chem. Phys.* **1956**, *25*, 467−478.
(51) Madjet, M. E.; Abdurahman, A.; Renger, T. *J. Phys. Chem. B* **2006**, *110*, 17268−17281.
(52) Sigfridsson, E.; Ryde, U. *J. Comput. Chem.* **1998**, *19*, 377−395.
(53) Krueger, B. P.; Scholes, G. D.; Fleming, G. R. *J. Phys. Chem. B* **1998**, *102*, 5378−5386.
(54) Hsu, C.-P.; You, Z.-Q.; Chen, H.-C. *J. Phys. Chem. C* **2008**, *112*, 1204−1212.
(55) Wang, M.; Silva, G. L.; Armitage, B. A. *J. Am. Chem. Soc.* **2000**, *122*, 9977−9986.
(56) Chowdhury, A.; Wachsmann-Hogiu, S.; Bangal, P. R.; Raheem, I.; Peteanu, L. A. *J. Phys. Chem. B* **2001**, *105*, 12196−12201.
(57) Chowdhury, A.; Yu, L.; Raheem, I.; Peteanu, L.; Liu, L. A.; Yaron, D. J. *J. Phys. Chem. A* **2003**, *107*, 3351−3362.
(58) Armitage, B. Cyanine Dye−Nucleic Acid Interactions. In *Heterocyclic Polymethine Dyes*; Strekowski, L., Ed.; Springer: Berlin, Germany, 2008; Vol. *14*, pp 11−29.
(59) Ziessel, R.; Harriman, A. *Chem. Commun.* **2011**, *47*, 611−631.
(60) Gonçalves, M. S. T. *Chem. Rev.* **2008**, *109*, 190−212.
(61) Champagne, B.; Guillaume, M.; Zutterman, F. *Chem. Phys. Lett.* **2006**, *425*, 105−109.
(62) Improta, R.; Santoro, F. *J. Chem. Theory Comput.* **2005**, *1*, 215−229.
(63) Schreiber, M.; Vahrenhorst, R.; Buss, V.; Fülscher, M. P. *Chirality* **2001**, *13*, 571−576.
(64) Send, R.; Valsson, O.; Filippi, C. *J. Chem. Theory Comput.* **2011**, *7*, 444−455.
(65) McRae, E. G.; Kasha, M. *J. Chem. Phys.* **1958**, *28*, 721−722.
(66) Cho, M.; Vaswani, H. M.; Brixner, T.; Stenger, J.; Fleming, G. R. *J. Phys. Chem. B* **2005**, *109*, 10542−10556.
(67) Brixner, T.; Stenger, J.; Vaswani, H. M.; Cho, M.; Blankenship, R. E.; Fleming, G. R. *Nature* **2005**, *434*, 625−628.
(68) Engel, G. S.; Calhoun, T. R.; Read, E. L.; Ahn, T.-K.; Mancal, T.; Cheng, Y.-C.; Blankenship, R. E.; Fleming, G. R. *Nature* **2007**, *446*, 782−786.
(69) Yoon, Z. S.; Yoon, M.-C.; Kim, D. *J. Photochem. Photobiol., C* **2005**, *6*, 249−263.
(70) Rudolph, M.; Autschbach, J. *J. Phys. Chem. A* **2011**, *115*, 2635−2649.
(71) Berova, N.; Di Bari, L.; Pescitelli, G. *Chem. Soc. Rev.* **2007**, *36*, 914−931.
(72) Cho, M. *Two-Dimensional Optical Spectroscopy*; CRC Press: Boca Raton, FL, 2009.
(73) Polavarapu, P. L. *J. Phys. Chem. A* **2005**, *109*, 7013−7023.